



REMOTE SENSING OF EVAPOTRANSPIRATION IN A SOUTHERN MEDITERRANEAN FOREST. APPLICATION TO BISSA FOREST, ALGERIA

Ababou Adda^{1†} — Chouieb Mohammed² — Saidi Djamel³ — Bouthiba Abdelkader⁴ — Mederbal Khalladi⁵

^{1,2}Biology Department, Faculty of Sciences, University Hassiba Ben Bouali, Chlef, Algeria

³Faculty of Science and engineering, University Ibn Badis, Mostaganem, Algeria

⁴Institute of Agronomical Sciences, University Hassiba Ben Bouali, Chlef, Algeria

⁵Faculty of Nature and Life Sciences, University Ibn Khaldoun, Tiaret, Algeria

ABSTRACT

The Simplified Surface Energy Balance Index (S-SEBI) algorithm was used in this study with four Landsat-5 Thematic Mapper images to assess the evapotranspiration (ET) in Bissa forest, one of the healthiest Algerian forests located south of the Mediterranean Sea. Results showed that ET varies over the different seasons, the highest ET values were reached during the spring due to water availability, whereas, the lowest values were recorded during the summer. The relationship between normalized difference vegetation index (NDVI) and ET showed that the highest ET values coincide always with the highest NDVI except for January where even the lowest NDVI values correspond to higher ET. The intensity of ET was closely related to aspects, southeastern exposures showed the highest ET, whereas, northwestern exposures showed the lowest ET.

Keywords: Algeria, Aspects, Bissa, Evapotranspiration, NDVI, Remote sensing, S-SEBI.

Received: 10 June 2016/ Revised: 10 July 2016/ Accepted: 25 August 2016/ Published: 8 September 2016

Contribution/ Originality

This study uses new estimation methodology of evapotranspiration, one of the most difficult climatic parameter to measure. Several classical approaches were developed to estimate evapotranspiration; in the opposite of these classical approaches we applied a new remote sensing algorithm to solve the energy balance equation in order to estimate evapotranspiration.

1. INTRODUCTION

Evapotranspiration (ET), referred to as a latent heat flux, is the most important mechanism of energy and mass exchange between hydrosphere, biosphere and atmosphere (Sobrino *et al.*, 2007; Nouri *et al.*, 2013). Evapotranspiration is controlled by several factors such as solar radiation, water availability, wind speed, soil characteristics and stomatal resistance (Roberts, 2000; Immerzeel *et al.*, 2006). Approximately 75% of the total precipitation are evapotranspired by the system soil-vegetation (Immerzeel *et al.*, 2006). Reliable estimation of temporal and spatial distribution of ET is at the basis of irrigation planning, land use and ecosystem management, especially in arid and semi-arid areas (Farias *et al.*, 2009; Liang *et al.*, 2010). In this context several classical approaches have been developed and used for decades to estimate ET, including temperature methods (Blaney and Criddle, 1950) radiation methods (Priestley and Taylor, 1972) and combination methods (Penman, 1948). Over the last decade, several remote sensing algorithms were developed (Bastiaanssen *et al.*, 1998) and applied to satellite imagery to solve the energy balance equation in order to estimate ET. The main advantage of this important

† Corresponding author

technological trend is that it can provide an estimation of ET at each point within a given area and provides its geographical distribution. Several energy balance algorithms using the thermal, visible bands and the formulation of the energy balance of the surface are available for calculating ET. In light of this, the Surface Energy Balance Algorithm for Land (SEBAL) (Bastiaanssen *et al.*, 1998) and the Simplified Surface Energy Balance Index (S-SEBI) (Roerink *et al.*, 2000) are among the most common remote sensing algorithms used to estimate the surface energy balance. The main difference between SEBAL and S-SEBI is that SEBAL needs the solution of a complex iterative process, while the S-SEBI algorithm, based on the latent heat flux and available energy to estimate the evapotranspiration; free it from all additional meteorological data. In this context the main purpose of this study was the use of the S-SEBI model combined with four Landsat images, to estimate the daily evapotranspiration (ET_d) according to the seasonal and topographical variation in a southern Mediterranean area characterized by its harsh climatic adversities.

2. MATERIAL AND METHODS

2.1. Study Area

Located in northwestern Algeria, the study area (Fig. 1) extends from 1°19'35" to 1°34'14" E, and from 36°22'29" to 36°30' 59" N, at 10 km away from the Mediterranean Sea and covers approximately 300 km² and. With a variable altitude ranging from 100 to 1120 m above the sea level, it's a typical Mediterranean area in terms of landscape structure, composition and climate, characterized by hot and dry summers, with a dry period of 4 months (May to September) and relatively rainy winters with an average annual rainfall of 500 mm. In terms of vegetation, the landscape is covered with natural sclerophyllous and sparse vegetation alternating with bare soils.



Fig-1. Location of the study area

2.2. S-SEBI Algorithm

Considering a natural surface the energy balance flux at the soil surface can be expressed according to Carson (1987) as:

$$R_n = G + H + \lambda ET \quad (1)$$

Where: where λET is the latent heat flux with λ as the latent heat of vaporization, R_n is the net radiation, G is the ground heat flux and H is the sensible heat flux.

To solve the surface energy balance flux (Eq. 1), the S-SEBI model (Roerink *et al.*, 2000) uses the evaporative fraction (Λ) (Eq. 2) (Table 1) based on the relationship between surface temperature (Eq. 3, Eq. 4 (NASA, 2009) Eq. 5 (Kosa, 2011)) and surface albedo (Eq. 6 (Liang *et al.*, 2003)) (Fig. 2). The instantaneous soil heat flux (G) was derived from an empirical equation proposed by Bastiaanssen (2000) and based on the relationship between normalized difference vegetation index (NDVI) and surface characteristics (Eq. 7 (Rouse *et al.*, 1974) and Eq. 8 (Tong *et al.*, 2007)) whereas the net radiation flux (R_n) was derived from Eq. 9 (Kosa, 2009) and Eq. 10 (Waters *et al.*, 2002). The sensible (H) and latent heat flux (λET) were calculated using Λ according to Eq. 11 and Eq. 12

(Roerink *et al.*, 2000). Finally, Eq. 13 and Eq. 14 (Namsik, 2010; Kosa, 2011) were used to estimate the daily (24 hours) evapotranspiration.

Table-1. Equations used to estimate the evapotranspiration from Landsat images.

Evaporative Fraction (Λ)	$\Lambda = (T_H - T_S)/(T_H - T_{\lambda E})$ (2)
Surface temperature ($^{\circ}K$)	1-Conversion of Digital numbers (DN) to radiance $L_{\lambda} = ((L_{max\lambda} - L_{min\lambda})/(QCAL_{max} - QCAL_{min})) \times (QCAL - QCAL_{min}) + L_{min\lambda}$ (3)
	2- Conversion of Landsat Thermal band 6 to effective at satellite temperature $T_{bb} = K_2 / \ln(K_1 / L_6 + 1)$ (4)
	3- Conversion of effective at satellite temperature to surface temperature $T_S = T_{bb} / \epsilon_0^{0.25}$ (5)
Albedo (α)	$\alpha_{Landsat} = 0.356 \times \rho_1 + 0.13 \times \rho_3 + 0.373 \times \rho_4 + 0.085 \times \rho_5 + 0.072 \times \rho_7 - 0.0018$ (6)
Soil Heat Flux (G) (W/m^2)	$NDVI = \rho_4 - \rho_3 / \rho_4 + \rho_3$ (7)
	$G/R_n = (T_s/\alpha) \times (0.0038 \times \alpha + 0.0074 \times \alpha^2) \times (1 - 0.98 \times NDVI^4)$ (8)
Net Radiation Flux (R_n) (W/m^2)	$\epsilon_0 = 1.009 + 0.047 \times \ln(NDVI)$ (9)
	$R_n = (1 - \alpha) \times R_s \downarrow + R_l \downarrow - R_l \uparrow - (1 - \epsilon_0) \times R_l$ (10)
Sensible Heat flux (H) (W/m^2)	$H = (1 - \Lambda) \times (R_n - G)$ (11)
Latent Heat flux (λET) (W/m^2)	$\lambda ET = \Lambda \times (R_n - G)$ (12)
Daily evapotranspiration ET_d ($mm/24h$)	$\Lambda_i = \Lambda_d = \lambda ET / (R_{ni} - G_i) = \lambda ET_d / (R_{nd} - G_d)$ (13)
	$ET_d = \lambda ET_i \times R_{nd} / \lambda R_{ni}$ (14)

Where: T_s = Land surface temperature; T_H and $T_{\lambda E}$ = Temperature of maximum sensible and latent heat flux; L_{λ} = Spectral radiance; $QCAL$ = quantized calibrated pixel value in DN; T_{bb} = Effective at satellite temperature; K_1 and K_2 are calibration constants = 666.09 and 1282.71 respectively; L_6 = spectral radiance for band 6; T_{bb} = Effective at satellite temperature; $\rho_{1,3,4,5,7}$ = Landsat reflectance bands; ϵ_0 = Surface emissivity; $R_s \downarrow$ = Incoming shortwave radiation; $R_l \downarrow$ = Incoming long wave radiation; $R_l \uparrow$ = Outgoing long wave radiation; G_d = Daily soil heat flux, it is approximately equal to zero (Allen *et al.*, 1998; Allen *et al.*, 2006).

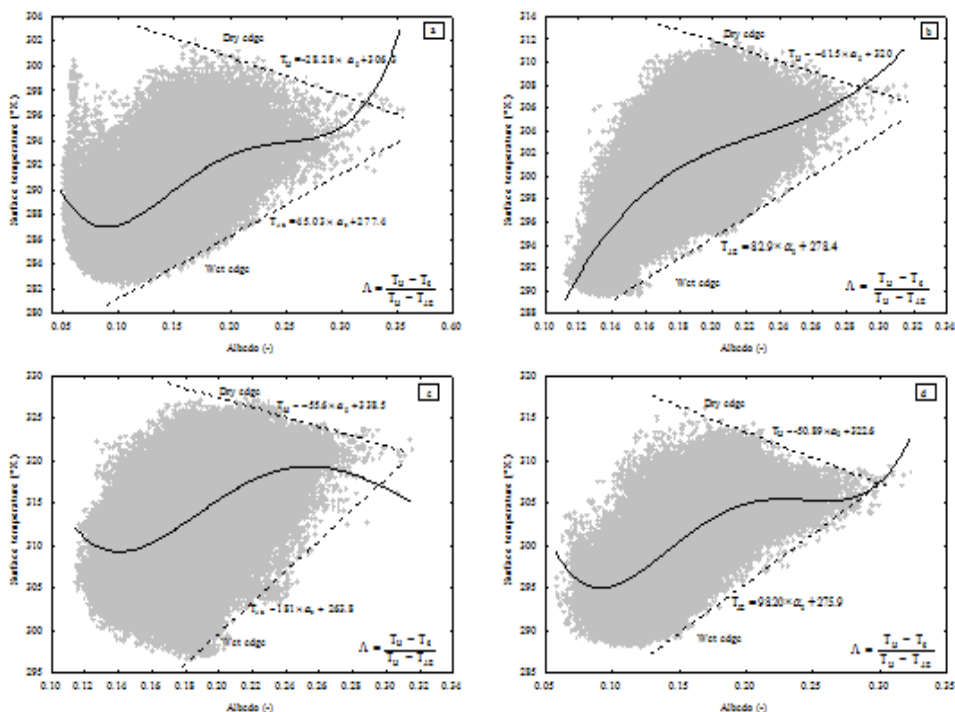


Fig-2. Surface temperature vs surface albedo (a) January, (b) April, (c) July, (d) October.

2.3. Aspects

Aspects of the study area were derived from a digital elevation model in a GIS. To underline the impact of aspects on ET_d , aspects were considered as circular form, with 8 directions, north-facing ($0-45^\circ$, $45-90^\circ$, $90-135^\circ$, $135-180^\circ$) and south-facing ($180-225^\circ$, $225-270^\circ$, $270-315^\circ$, $315-360^\circ$)

3. RESULTS AND DISCUSSIONS

3.1. Spatiotemporal variation of ET_d

Unlike all the empirical and recent remote sensing models which require a lot of local meteorological data, the S-SEBI model used in this study was based on relatively low information input, just visible, near infrared, thermal bands (used to extract surface temperature and reflectance (albedo)) and incoming radiation on the ground, it showed an easy applicability and high accuracy for the retrieval of ET_d using remotely sensed information, according to [Sobrino *et al.* \(2005\)](#) the accuracy for the ET_d estimated using the S-SEBI model was found to be less than 1 mm/d compared to the measured ET. As a result, the spatial distribution of ET_d in Bissa forest using Landsat images showed that there was a wide spatial variation in ET, the maps generated through the S-SEBI algorithm (Fig. 3) revealed that ET_d was highly variable according to season and land vegetation cover, these observations were consistent with those reported by ([Dolan *et al.*, 1984](#); [Courault and Monestiez, 1999](#); [Aleina *et al.*, 2013](#)). Throughout the study area, according to land vegetation cover, the highest ET_d was observed over dense forest canopy and the lowest was recorded over bare soils.

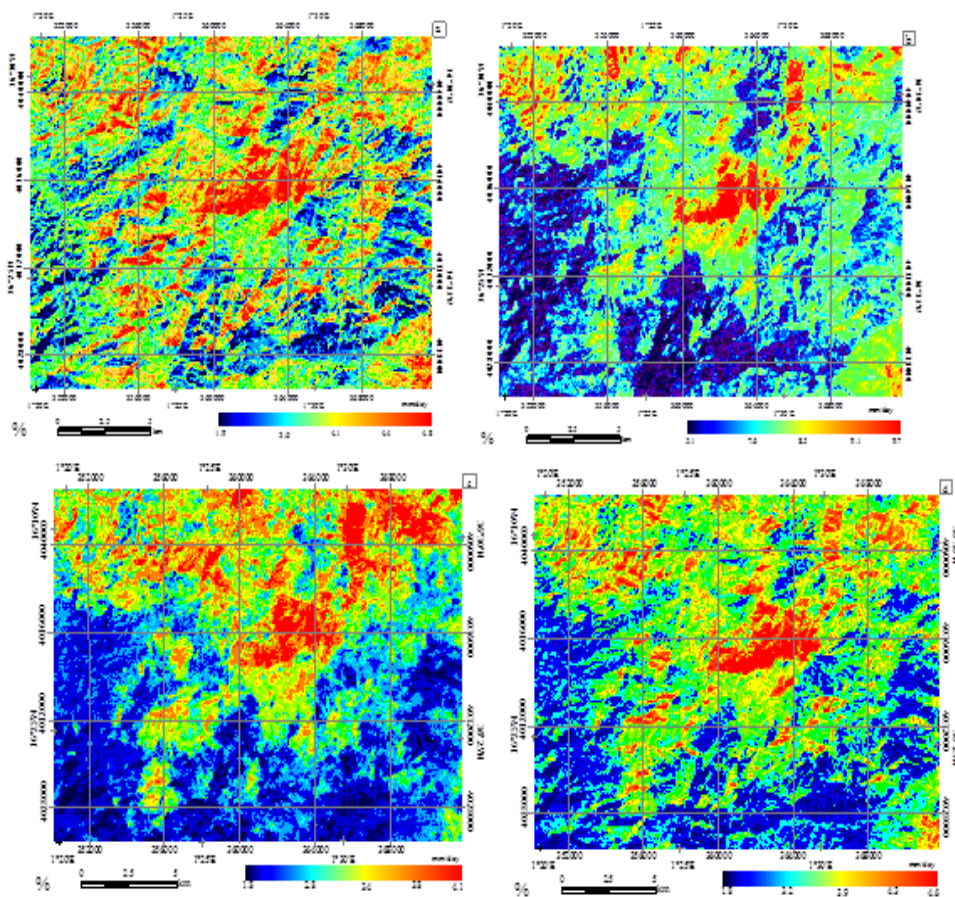


Fig-3. Spatial distribution of ET_d (a) January, (b) April, (c) July, (d) October.

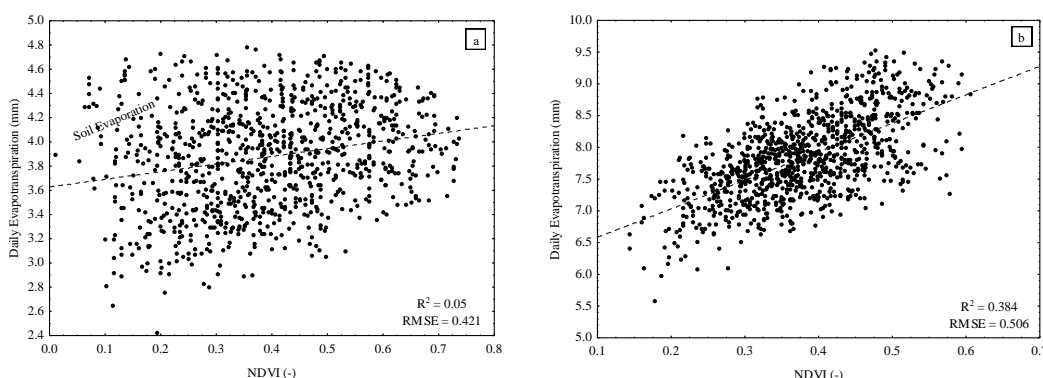
Whereas, according to season, due to water availability, spring (Fig. 3b) showed the highest mean ET_d (7.97 mm), the widest spatial variation within a range from 5.1 to 9.7 mm and the highest standard deviation (0.624) (Table 2). As Mediterranean summers are very hot and strongly dry (Mean Temperature = $41\text{ }^\circ\text{C} \pm 5.6\text{ }^\circ\text{C}$ during image capture), the lowest mean ET_d (3.17 mm), the narrowest range (1.8 to 4.1 mm) and the weakest standard deviation (0.36) were observed during July (Fig. 3c) due to vegetation resistance to drought and water scarcity. Winter and autumn (Fig. 3a and Fig. 3d) were comparable in term of daily mean ET, spatial variation and standard deviation (Table 2).

Table-2. Summary of descriptive statistics of ET_d during the four months

	January	April	July	October
Minimum	1.873	5.102	1.835	1.848
Maximum	4.839	9.671	4.108	4.639
1st Quartile	3.582	7.543	2.905	3.331
3rd Quartile	4.213	8.389	3.447	3.859
Mean	3.885	7.969	3.171	3.589
Standard deviation (σ)	0.427	0.624	0.362	0.387

3.2. Relationship between ETD and NDVI

In general, it was remarked that the highest ET values coincide always with the highest NDVI, except winter (January) where even the lowest NDVI values correspond to higher ET_d , with a weak coefficient of determination (R^2) equal to 0.05, this behaviour was closely related to the existence of intense bare soil evaporation beside vegetation transpiration, which reflects the availability of water during this season, indeed the total rainfall accounted during the 60 days preceding the image capture was more than 150 mm. The strongest ET-NDVI correlation was observed during summer (July) with a coefficient of determination (R^2) equal to 0.65 (Fig. 4c) suggesting that 65% of the ET_d variability was explained by the NDVI, moreover, during this season was recorded the lowest root mean square error (RMSE) (0.228), which reflects the fact that the evapotranspiration process was strictly limited to vegetation transpiration, and almost a total absence of soil evaporation due to the scarcity of rainfall during this season, the amount of rainfall recorded during the 2 months preceding the image capture was less than 15 mm, this July relationship (NDVI-ET) was also reported by Krishnan *et al.* (2012) thus, in contrary to Nicholson *et al.* (1996) and Szilagyi *et al.* (1998) who pointed out that the NDVI-ET relationship is strong, mainly, in humid environments, our results showed an increasing relationship (NDVI-ET) with the growing aridity of the environment. This difference is probably due to the nature of local climate and vegetation. Our findings were very concordant with the Mediterranean climate, as reported by many authors (Sumner *et al.*, 2001; Blumler, 2005; Li *et al.*, 2006) the Mediterranean climate is characterized by its strong seasonal contrast, with hot dry summers and cool rainy winters.



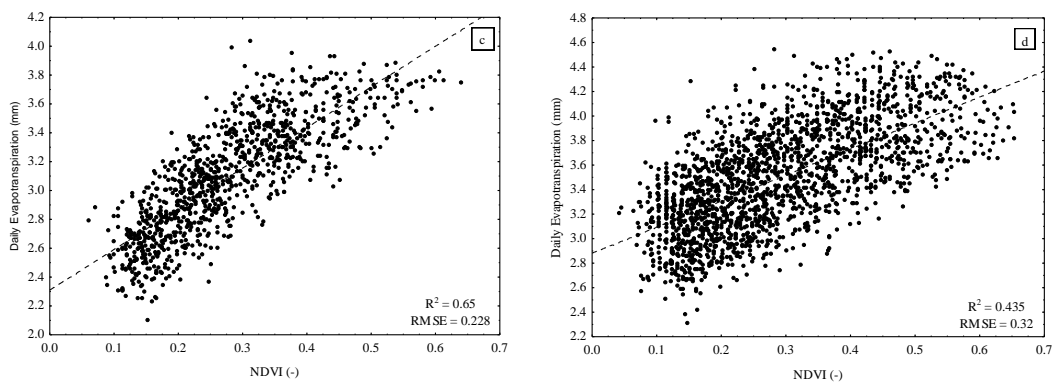


Fig-4. ET_d (mm) vs NDVI (a) January, (b) April, (c) July, (d) October

Compared to summer, spring (April) and autumn (October) (Fig. 5b and 5d) showed a relatively low R^2 equal to almost 0.4 for both seasons, nevertheless this 40% of ET_d variability explained by NDVI was highly significant ($P < .001$) according to the linear regression analysis.

3.3. Variations of Etd According to Aspects

As ET depend on many aspects of the local geographical and physiographical conditions, which need to be accounted in ET estimation, results showed that the intensity of ET_d was closely related to aspects and consequently negatively related to shade (Fig. 5), this finding was also reported by Tong *et al.* (2007). Winter and autumn (Fig. 5a and 5d) showed almost the same behaviour according to aspects, the lowest ET_d (3.40 and 3.26 mm, respectively) was observed in the direction 135-180°, whereas the highest ET_d (4.33 and 3.90 mm, respectively) was shown by the opposite side, i.e., 315 - 360°. The highest negative correlation between ET_d and shade was recorded during these two seasons with a coefficient of correlation (R) equal to - 0.65 ($P < .001$) during winter and - 0.53 ($P < .001$) during autumn (Table 3). Throughout spring period (April) the ET-shade correlation was slightly low ($R = - 0.4$), over this season ET_d was the highest at the direction 270 - 360°, whereas the lowest ET_d was recorded at the opposite exposure 90 - 180° (Fig. 5b), with a slightly large sector of circle of 90° compared to winter and autumn (45°). Finally, the lowest ET-shade correlation ($R = - 0.29$) was recorded during the dry season (summer), regarding ET_d the lowest and the highest values were recorded at the respective directions 90 - 225° and 270 - 45°, with the largest sector of circle of 135°. This high variability of ET_d according to aspects was related to the amount of sunshine received by each aspect at the moment of image capture (10 H: 20 MN), southerly aspects tends to be more sunny than on northerly aspects, this fact was confirmed by the inverse relationship observed between ET_d and shade, where, it was also noted that this negative correlation increases when the sector of circle width's decreases and vice versa. Therefore, ET_d calculation at different hours of the day is necessary in order to accurately assess ET_d throughout the different seasons, unfortunately we note the unavailability of satellite imagery captured throughout the different times of the day.

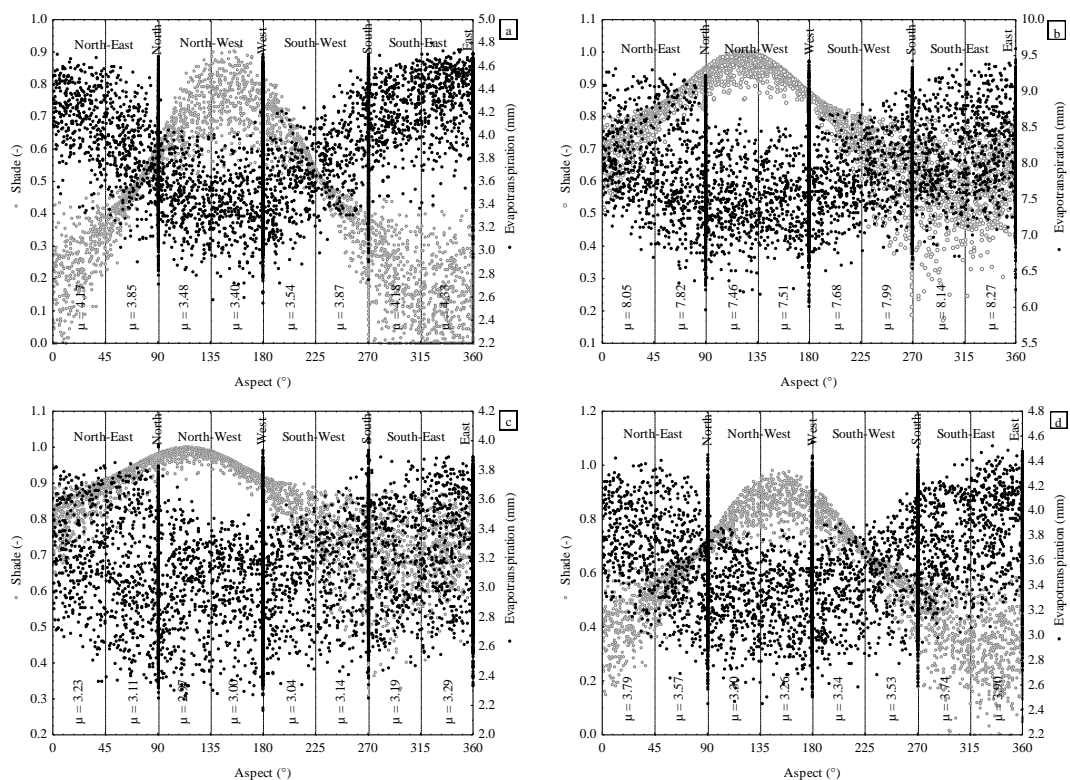


Fig-5. ET (mm) vs aspects and shade (a) January, (b) April, (c) July, (d) October

Table-3. Results of regression analysis between ET_d (mm) and shade (-)

	January	April	July	October
R	-0.65	-0.4	-0.290	-0.530
R ²	0.423	0.16	0.082	0.277
RMSE	0.334	0.573	0.341	0.333
P	< .001	< .001	< .001	< .001

Comparing the mean ET_d recorded at the different range of aspects during the four seasons, analysis of variance (ANOVA), resulted in different groups of ET_d highly significantly different ($P < .001$) according to aspects (Table 4), which reflects the high influence of the local geographic and physiographic conditions on evapotranspiration, concurring with the findings reported by many authors (Jackson, 1967; Toy, 1979; Stephenson, 1998).

Table-4. Different groups of ET_d related to aspects according to ANOVA and Tukey (HSD) (a) January, (b) April, (c) July, (d) October.

Aspect (°)	January					April					July					October				
	Groups					Groups					Groups					Groups				
	G1	G2	G3	G4	G5	G1	G2	G3	G4	G5	G6	G1	G2	G3	G4	G1	G2	G3	G4	G5
0-45		B					B	C				A	B				B			
45-90			C						D					C				C		
90-135				D							F				D				D	E
135-180					E						F				D					E
180-225				D						E					D					D
225-270			C					C					C					C		
270-315		B					B						B	C			B			
315-360	A					A						A				A				

*G = group

4. CONCLUSION

As ET is at the basis of irrigation planning, land use and ecosystem management, quantification of ET has been for decades a constant concern of farmers and researchers. Among several approaches, this study focused on the estimation of ET through remote sensing. Despite the simplicity and the low input data required by this technique, it was possible to accurately estimate the daily evapotranspiration with its spatiotemporal distribution in a southern Mediterranean forest, the highest ET_d were reached during the spring due to water availability, whereas, the lowest values were recorded during the summer. Regarding the influence of vegetation, the highest ET_d were always related to the highest NDVI, except for January where even the lowest NDVI corresponded to higher ET_d . It was also found that the intensity of ET_d was closely related to the local topographical and physiographical conditions, south-eastern exposures showed the highest ET_d , whereas, north-western exposures were characterized by the lowest ET_d . Finally, the outcomes of this study confirm the promising possibilities of remote sensing in solving the energy balance equation and accurately assess the spatial and the temporal variation of ET.

Funding: This study received no specific financial support.

Competing Interests: The authors declare that they have no competing interests.

Contributors/Acknowledgement: All authors contributed equally to the conception and design of the study.

REFERENCES

- Aleina, F.C., M. Baudena, F. Andrea and A. Provenzale, 2013. Multiple equilibria on planet Dune: Climate-vegetation dynamics on a sandy planet. *Tellus B, Chemical and Physical Meteorology*, 65(17662): 1-12.
- Allen, R.G., L.S. Pereira, D. Raes and M. Smith, 1998. Crop evapotranspiration: Guidelines for computing crop water requirements FAO irrigation and drainage. Paper No 56, Rome-Italy. Available from <http://www.fao.org/docrep/X0490E/x0490e00.htm> [Accessed 25 January 2015].
- Allen, R.G., R. Trezza and M. Tasumi, 2006. Analytical integrated functions for daily solar radiation on slopes. *Agricultural and Forest Meteorology*, 139(2): 55-73.
- Bastiaanssen, W.G.M., 2000. SEBAL-based sensible and latent heat fluxes in the irrigated Gediz Basin, Turkey. *Journal of Hydrology*, 229(2): 87-100.
- Bastiaanssen, W.G.M., M. Menenti, R.A. Feddes and A.A.M. Holtslag, 1998. A remote sensing surface energy balance algorithm for land (SEBAL): 1. Formulation. *J. Hydrol*, 212(213): 198-212.
- Blaney, H.F. and W.D. Criddle, 1950. Determining water requirements in irrigated areas from climatological irrigation data. USDA, Soil Conservation Service, Technical Paper N° 96, Washington, D.C.
- Blumler, M.A., 2005. Three conflated definitions of mediterranean climates. *Middle States Geographer*, 38(1): 52-60.
- Carson, D.J., 1987. An introduction to the parameterization of land surface processes: Part 1. Radiation and turbulence. *Meteorological Magazine*, 116(1): 229-242.
- Courault, D. and P. Monestiez, 1999. Spatial interpolation of air temperature according to atmospheric circulation patterns in the South-East of France. *International Journal of Climatology*, 19(4): 365-378.
- Dolan, T.J., A.J. Hermann, S. Bayley and J. Zoltek, 1984. Evapotranspiration of a Florida, U.S.A., freshwater wetland. *Journal of Hydrology*, 74(4): 355-371.
- Farias, O.S., S. Irmak and R.H. Cuenca, 2009. Special issue on evapotranspiration measurement and modeling. *Irrigation Science*, 28(1): 1-3.
- Immerzeel, W.W., P. Droogers and A. Gieske, 2006. Remote sensing and evapotranspiration mapping: State of the art. *Future Water Report 55*. Research Paper N°1, Wageningen, Netherlands.
- Jackson, R.J., 1967. The effect of slope, aspect and albedo on potential evapotranspiration from hill- slopes and catchments. *NZ Journal of Hydrology*, 6(1): 60-69.

- Kosa, P., 2009. Air temperature and actual evapotranspiration correlation using landsat 5 tm satellite imagery. *Kasetsart Journal (Natural Science)*, 43(3): 605-611.
- Kosa, P., 2011. The effect of temperature on actual evapotranspiration based on landsat-5 TM satellite imagery, Chapter 9. In: *Evapotranspiration*, Leszek Labeledzki (Ed.), Intech Publisher. pp: 209-228.
- Krishnan, P., T.P. Meyers, R.L. Scott, L. Kennedy and M. Heuer, 2012. Energy exchange and evapotranspiration over two temperate semi-arid grasslands in North America. *Agricultural and Forest Meteorology*, 153(2): 31-44.
- Li, L., A. Bozec, S. Somot, K. Beranger, P. Bouruet-Aubertot, F. Sevault and M. Crepon, 2006. Regional atmospheric, marine processes and climate modeling. In: Lionello P, Malanotte-Rizzoli P, Boscolo R, Editors. *Mediterranean climate variability, developments in earth and environmental sciences*, 4(1): 373-397.
- Liang, L., L. Li and Q. Liu, 2010. Spatial distribution of reference evapotranspiration considering topography in the Taoer river basin of Northeast China. *Hydrology Research*, 41(5): 424-437.
- Liang, S., C.J. Shuey, A.L. Russ, H. Fang, M. Chen, C.L. Walthall, C.S.T. Daughtry and J.R. Hunt, 2003. Narrowband to broadband conversions of land surface albedo: II. Validation. *Remote Sensing of Environment*, 84(5): 25-41.
- Namsik, P., 2010. *Advances in geosciences: Hydrological science (Hs)*. World Scientific Publishing Company, Incorporated, 17: 458.
- NASA, 2009. Landsat 7 Science data user's handbook is a living document prepared by the landsat project science office at NASA's goddard space flight center in greenbelt, Maryland. Available from http://landsathandbook.gsfc.nasa.gov/pdfs/Landsat7_Handbook.pdf [Accessed 12 January 2015].
- Nicholson, S.E., A.R. Lare, J.A. Marengo and P. Santos, 1996. A revised version of lettaus evapoclimatology model. *Journal of Applied Meteorology*, 35(4): 549-561.
- Nouri, H., S. Beecham, F. Kazemi, A.M. Hassanli and S. Anderson, 2013. Remote sensing techniques for predicting evapotranspiration from mixed vegetated surfaces. *Hydrology and Earth System Sciences Discussions*, 10(3): 3897-3925.
- Penman, H.L., 1948. Natural evaporation from open water, bare soil and grass. *Proceedings of the Royal Society A, London*, 193(1032): 120-145.
- Priestley, C.H.B. and R.J. Taylor, 1972. On the assessment of the surface heat flux and evaporation using large-scale parameters. *Monthly Weather Review*, 100(2): 81-92.
- Roberts, J., 2000. The influence of physical and physiological characteristics of vegetation on their hydrological response. *Hydrological Processes*, 14(17): 2885-2901.
- Roerink, G.J., Z. Su and M. Menenti, 2000. S-SEBI: A simple remote sensing algorithm to estimate the surface energy balance. *Physics and Chemistry of the Earth Part B Hydrology Oceans and Atmosphere*, 25(2): 147-157.
- Rouse, J.W., R.H. Haas, J.A. Schell and D.W. Deering, 1974. Monitoring vegetation systems in the great plains with ERTS. In: Fraden SC, Marcanti EP, Becker MA, Editors, *Third ERTS-1 Symposium*, Washington DC, NASA.
- Sobrino, J.A., M. Gomez, J.C. Jimenez-Munoz and A. Olivos, 2007. Application of a simple algorithm to estimate daily evapotranspiration from NOAA-AVHRR images for the Iberian Peninsula. *Remote Sensing of Environment*, 110(2): 139-148.
- Sobrino, J.A., M. Gómez, J.C. Jimenez-Munoz, A. Olivos and G. Chehbouni, 2005. A simple algorithm to estimate evapotranspiration from DAIS data: Application to the DAISEX campaigns. *Journal of Hydrology*, 315(4): 117-125.
- Stephenson, N., 1998. Actual evapotranspiration and deficit: Biologically meaningful correlates of vegetation distribution across spatial scales. *Journal of Biogeography*, 25(5): 855-870.
- Sumner, G., V. Homar and C. Ramis, 2001. Precipitation seasonality in Eastern and Southern coastal Spain. *International Journal of Climatology*, 21(2): 219-247.
- Szilagyi, J., D.C. Rundquist, D.C. Gosselin and M.B. Parlange, 1998. NDVI relationship to monthly evaporation. *Geophysical*

Research Letters, 25(10): 1753-1756.

Tong, L., S.Z. Kang and L. Zhang, 2007. Temporal and spatial variations of evapotranspiration for spring wheat in the Shiyang River Basin in Northwest China. *Agricultural Water Management*, 87(3): 241–250.

Toy, T.J., 1979. Potential evapotranspiration and surface-mine rehabilitation in the Powder river Basin, Wyoming and Montana. *Journal of Range Management*, 32(4): 312-317.

Waters, R., R. Allen and W. Bastiaanssen, 2002. SEBAL. Surface energy balance algorithms for Land.Idaho Implementation. Idaho, USA: Advanced Training and User's Manual.

Views and opinions expressed in this article are the views and opinions of the author(s), The International Journal of Biotechnology shall not be responsible or answerable for any loss, damage or liability etc. caused in relation to/arising out of the use of the content.